# LETTER

# Rapid coupling between ice volume and polar temperature over the past 150,000 years

K. M. Grant[1], E. J. Rohling[1,2], M. Bar-Matthews[3], A. Ayalon[3], M. Medina-Elizalde[1]†, C. Bronk Ramsey[4], C. Satow[5] & A. P. Roberts[2]

Current global warming necessitates a detailed understanding of the relationships between climate and global ice volume. Highly resolved and continuous sea-level records are essential for quantifying ice-volume changes. However, an unbiased study of the timing of past ice-volume changes, relative to polar climate change, has so far been impossible because available sea-level records either were dated by using orbital tuning or ice-core timescales, or were discontinuous in time. Here we present an independent dating of a continuous, high-resolution sea-level record[1,2] in millennial-scale detail throughout the past 150,000 years. We find that the timing of ice-volume fluctuations agrees well with that of variations in Antarctic climate and especially Greenland climate. Amplitudes of ice-volume fluctuations more closely match Antarctic (rather than Greenland) climate changes. Polar climate and ice-volume changes, and their rates of change, are found to covary within centennial response times. Finally, rates of sea-level rise reached at least 1.2 m per century during all major episodes of ice-volume reduction.

During the past few million years, variability in global ice volume (sea level) has been one of the main feedback mechanisms in climate change (see, for example, refs 3, 4). However, detailed assessment of the role of ice volume in climate change is hindered by inadequacies in sea-level records and/or their chronologies. First, dated coral sea-level benchmarks are discontinuous before the last glacial maximum (LGM; ~22,000 years ago). Second, continuous sea-level records have insufficient chronological control; they rely on orbital tuning, correlations with ice-core records, or imperfect transfer of coral datings[1,2,5–7]. Orbital tuning assumes a systematic response between changes in ice volume and Earth's orbital parameters, so that the relationship between insolation forcing and global ice volume cannot be discerned from orbitally tuned records. In addition, the timing of any centennial-scale to millennial-scale fluctuations in ice volume will be poorly constrained in orbitally tuned sea-level records because the shortest orbital frequency is ~19,000 years. Transferring an ice-core chronology to a sea-level record requires an assumption that ice volume always varies in a systematic phase relationship with either Antarctic or Greenland climate, which may not be the case (see, for example, refs 1, 2, 8, 9).

We resolve these issues for the past 150,000 years using a novel approach to provide a detailed chronology to the continuous and highly resolved record of Red Sea relative sea-level (RSL)[2]. We exploit a 'basin isolation' concept, similar to that used for the Red Sea[1,2], in the nearby eastern Mediterranean, where marine sediments can be dated much more accurately. Because the hydrological cycle directly links the $\delta^{18}O$ of eastern Mediterranean surface waters and that of cave speleothems on bordering land masses downwind of this highly evaporative sea[10,11], we can directly relate our new high-resolution planktonic foraminiferal $\delta^{18}O$ record for the surface-dwelling species *Globigerinoides ruber* (white form) in eastern Mediterranean sediment core LC21 ($\delta^{18}O_{ruber}$) to the U–Th-dated Soreq Cave speleothem $\delta^{18}O$ record ($\delta^{18}O_{speleo}$) (Fig. 1; Methods and Supplementary Information).

Previous work demonstrated quantitatively that eastern Mediterranean $\delta^{18}O$ has a strong overprint of sea-level variability[12]; hence, considerable agreement is expected between $\delta^{18}O$ signals for the Red Sea and the eastern Mediterranean (Supplementary Information). Although the more complicated hydrological cycle in the Mediterranean (relative to the Red Sea) means that variations in eastern Mediterranean $\delta^{18}O$ cannot be used to determine the amplitudes of sea-level change precisely, the basin isolation effect imposes sufficient $\delta^{18}O$ signal similarity between the two seas to allow accurate transfer of the superior eastern Mediterranean chronology to the Red Sea record. This is achieved using our new $\delta^{18}O$ record from core LC21 for the subsurface-dwelling planktonic foraminifer *Neogloboquadrina pachyderma* (dextral) ($\delta^{18}O_{pac}$), which is known to minimize surface-water $\delta^{18}O$ overprints (Fig. 1, Methods and Supplementary Information).

Construction of the new RSL chronology involves two stages. First, we build an age model for eastern Mediterranean core LC21 by correlating its $\delta^{18}O_{ruber}$ record with the Soreq Cave $\delta^{18}O_{speleo}$ record over the interval 40–160 kyr BP (Fig. 1a and Supplementary Information). For the interval 0–40 kyr BP, our age model is constrained by 14 radiocarbon datings and two well-documented and independently dated tephra horizons from the Minoan[13] and Campanian Ignimbrite (CI)[14] eruptions. A Bayesian depositional model (constructed using OxCal[15]) comprising the original Soreq Cave chronology, the $^{14}C$ datings and the chronostratigraphic position of all Soreq–LC21 tie-points (Supplementary Information) then improves the accuracy of the Soreq Cave chronology and $^{14}C$ datings, and consequently that of core LC21, and rigorously determines the chronological uncertainties of the LC21 tie-points. Next, we transfer the new LC21 age model to the RSL record between 22,000 and 150,000 years ago using the $\delta^{18}O_{pac}$ record (Fig. 1b; Supplementary Information). For the younger interval (0–22,000 years ago), we correlate RSL with a recent sea-level probability curve based on radiometrically dated sea-level benchmarks[16]; this is a more direct correlation target than $\delta^{18}O_{speleo}$ for this interval (Fig. 1b). Our correlations reveal that Last Interglacial (LIG) sea levels peaked before the main (monsoonal) wet phase in the eastern Mediterranean (Fig. 1b). This is stratigraphically corroborated within Red Sea core KL09, in which runoff-related soil biomarkers appear after the LIG highstand signal[17] (Fig. 1b).

Age uncertainties are quantified for all correlations to allow full error propagation into the new RSL chronology. A root-mean-squares estimate at the 95% ($2\sigma$) probability level is calculated that fully accounts for errors associated with sample-spacing in the $\delta^{18}O_{speleo}$, $\delta^{18}O_{ruber}$, $\delta^{18}O_{pac}$ and RSL records, as well as the analytical error associated with the Soreq Cave U–Th and LC21 $^{14}C$ datings, and the $2\sigma$ confidence interval of the sea-level probability curve (Supplementary Information). We reinforce this by categorizing our chosen tie-points into three levels of confidence: category 1 is considered the most reliable and within the bounds of sample-spacing, category 2 tie-points may be moved by $\pm0.5$ kyr, and category 3 tie-points are the most

[1]School of Ocean and Earth Science, University of Southampton, National Oceanography Centre, European Way, Southampton SO14 3ZH, UK. [2]Research School of Earth Sciences, The Australian National University, Canberra, ACT 0200, Australia. [3]Geological Survey of Israel, 30 Malchei Israel Street, Jerusalem 95501, Israel. [4]Research Laboratory for Archaeology and the History of Art, Dyson Perrins Building, University of Oxford, South Parks Road, Oxford OX1 3QY, UK. [5]Department of Geography, Queens Building, Royal Holloway University of London, Egham, Surrey TW20 0EX, UK. †Present address: Centro de Investigación Científica de Yucatán, Unidad Ciencias del Agua, Calle 8, No. 39, Mz. 29, S.M. 64 Cancun, Quintana Roo, CP 77500, México.
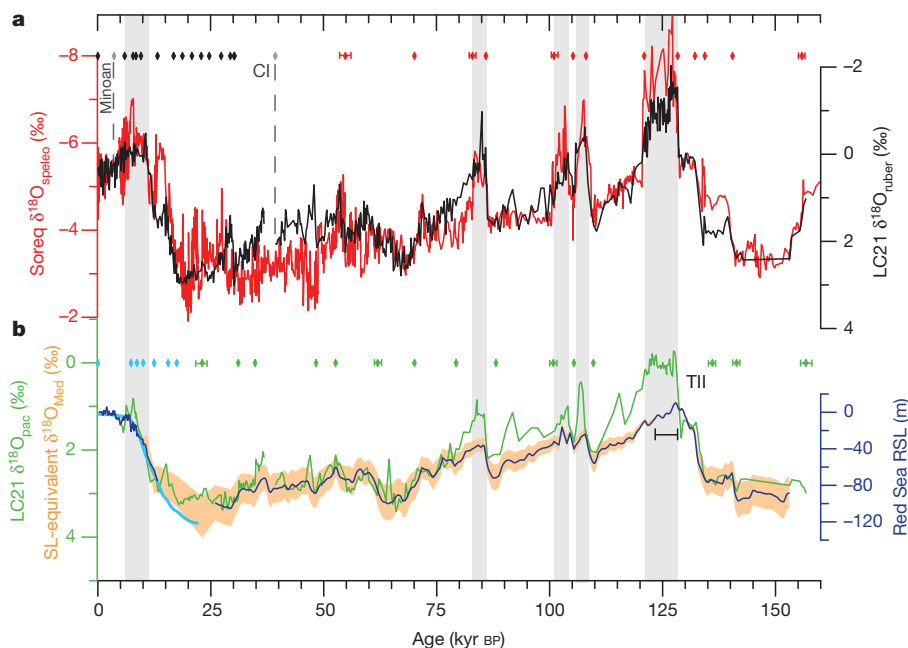
**Figure 1 | Correlation of Soreq Cave and eastern Mediterranean (LC21) $\delta^{18}O$ signals and the Red Sea RSL record. a,** New planktonic foraminiferal (*G. ruber*) $\delta^{18}O_{ruber}$ record from core LC21 (black), Soreq Cave $\delta^{18}O_{speleo}$ record (red) (Supplementary Information) and tie-points (red diamonds) used to correlate the LC21 and Soreq Cave records. Error bars ($\pm0.5$ and $\pm1$ kyr) denote more ambiguous tie-points (Supplementary Information). Also indicated are $^{14}C$ datings (black diamonds), the Minoan and Campanian Ignimbrite (CI) tephra horizons (dashed black lines) and intervals of sapropel deposition (grey rectangles). **b,** Red Sea RSL record[2] (dark blue, 1-kyr moving

Gaussian filter) after correlation with the LC21 (*N. pachyderma*) $\delta^{18}O_{pac}$ record (green) and with a highest-probability sea-level curve[16] (light blue). Correlation tie-points (green and light blue diamonds, with error bars as in **a**) and termination II (TII) are indicated. For a Mediterranean $\delta^{18}O$ ($\delta^{18}O_{Med}$) enrichment of $2.5 \pm 0.5$‰ per 120 m sea-level change[12], RSL was converted into equivalent $\delta^{18}O_{Med}$ values (orange shading). A LIG wet phase in the Red Sea (about 124–128 kyr BP; black bar) is also indicated[17]. RSL is not reliable for about 14–23 kyr BP because of an aplanktonic zone in Red Sea sediments (Supplementary Information).

contentious and may be moved by $\pm1$ kyr (Fig. 1). On the basis of the total error of each RSL tie-point, we interpolate a $2\sigma$ age uncertainty for every data point in the RSL record (Supplementary Information). Finally, these age uncertainties are combined with methodological sea-level uncertainties ($\pm12$ m at the $2\sigma$ level[1]) in a probabilistic assessment of the RSL record (Fig. 2 and Supplementary Information). This reveals that, during the LIG, RSL at Hanish sill (gateway to the Red Sea) stood above 0 m at 126–130 or 120–133 kyr BP (95% confidence limits to the maximum-probability RSL (RSL$_{Pmax}$) and RSL data points, respectively), and peaked at 127–129 or 126–132 kyr BP (95% confidence limits to RSL$_{Pmax}$ and RSL data points, respectively; Fig. 2). Although the depth of Hanish sill is implicit in the Red Sea sea-level method, the timing and magnitude of LIG sea levels in our RSL record may be expected to differ from eustatic sea level (ESL) as a result of isostatic effects at the sill[18]; our datings are therefore likely to be refined by detailed isostatic modelling of the sill.

We now compare our probabilistic sea-level curve with other key records of sea level and high-latitude climate (Fig. 2). Our new RSL record agrees well—within uncertainties—with coral sea-level benchmarks (Fig. 2b). Discrepancies in Marine Isotope Stages 5e and 5a may relate to uncertainties in coral position or depth habitat, tectonic/isostatic effects among sites, and/or isostatic effects at Hanish sill[18].

In general, our sea-level record agrees well with variability in ice volume suggested by deep-sea benthic foraminiferal $\delta^{18}O$, and with the major (orbital-scale) climate transitions recorded in Greenland and Antarctic ice cores (Fig. 2). Exceptions to this broad coherence are termination I in the benthic foraminiferal $\delta^{18}O$ record[5] of marine core MD95-2042 from the Iberian margin (Fig. 2d), and termination II and the Marine Isotope Stages 4–3 transition in a global benthic $\delta^{18}O$ stack[19] (Fig. 2c). Given that RSL agrees well with all other proxy records over these transitions, we surmise that these offsets are due to orbital tuning, lower sample resolution[19] and potential bias from deep-sea temperature changes[5] and isostatic effects.

Given that the eustatic glacial–interglacial sea-level range is implicitly accounted for in the Red Sea sea-level method, RSL is a good approximation of variations in ESL (ice volume)[1], although it may underestimate ESL variability by as much as 10% (ref. 18). Regarding polar climate variations, the structure and amplitude of Antarctic climate variations agree well with the record of highest-probability ice-volume fluctuations (Fig. 2e). This corroborates previous observations[1,2,5] but, crucially, is more conclusive because our new chronology is entirely independent of ice-core age models. The Antarctic–RSL relationship is most tenuous at about 95–115 kyr BP, at which RSL instead agrees better with Greenland climate fluctuations. Indeed, the timing of ice-volume changes is generally found to be close to that of Greenland climate variability (Fig. 2f). However, higher-amplitude Greenland $\delta^{18}O$ oscillations ('Dansgaard–Oeschger' events[20]) generally exceed concomitant ice-volume variability. In summary, at the maximum probability and 95% confidence levels for RSL, the timing and structure of large-scale sea-level variability reflects a global signature of climate changes recorded in both Antarctic and Greenland ice cores.

Phase relationships between changes in polar climate and ice volume are initially evaluated by lagged correlations between the ice-core data (European Project for Ice Coring in Antarctica (EPICA) Dronning Maud Land (EDML) $\delta^{18}O$ and North Greenland Ice-core Project (NGRIP) $\delta^{18}O$) and RSL (Supplementary Information). We find that ice-volume lags of 100–400 and 200–400 years produce the best correlations with Antarctic and Greenland climate changes, respectively (Fig. 3a, b and Supplementary Information). Rates of change in ice volume and in polar climate correlate most strongly within $\pm200$ years (Fig. 3a, b). Further assessment with cross-spectral analyses of the EDML $\delta^{18}O$, NGRIP $\delta^{18}O$, and RSL records (and their derivatives) confirms that, for suborbital frequencies, peak coherences between Greenland climate and ice volume are associated with minimal phase offsets ($\pm300$ years), whereas phase offsets between Antarctic temperature and ice volume are potentially larger (400–700 years;
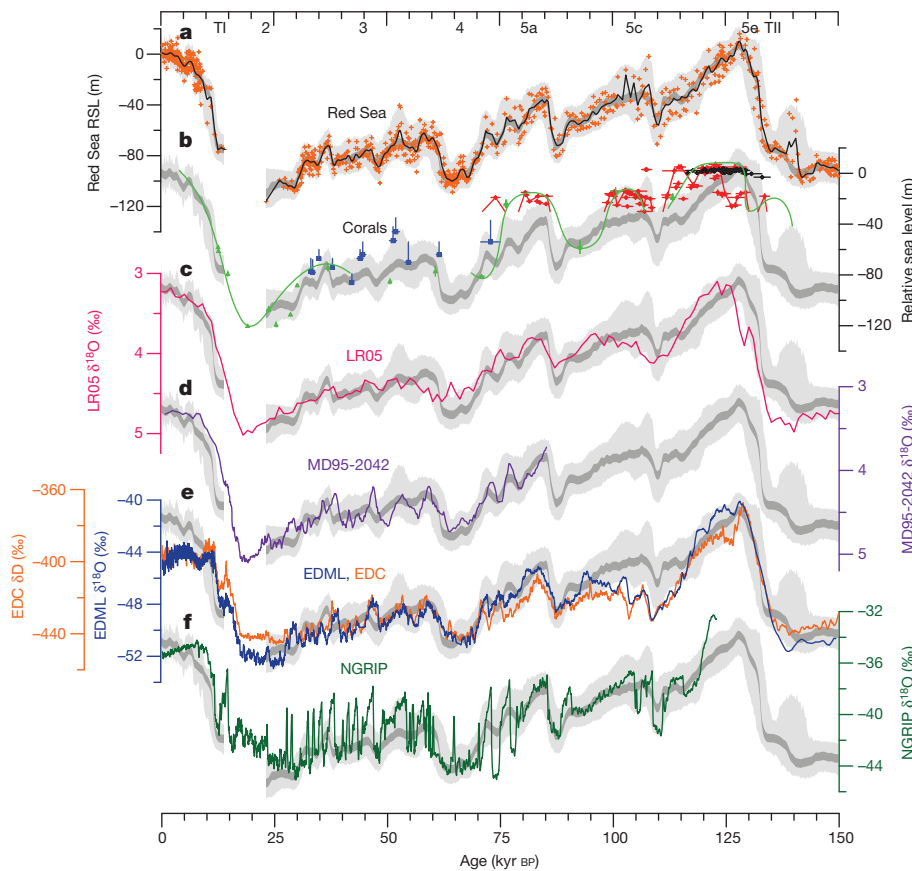
**Figure 2 | Comparison of probabilistic assessment of RSL with other sea-level reconstructions and with Antarctic and Greenland climate variability.** Confidence intervals of 95% for the RSL data (light grey) and probability maximum (dark grey) (Supplementary Information) are superimposed on: **a**, Red Sea RSL data on our new chronology (orange crosses; black line, 1 kyr moving Gaussian filter); **b**, coral sea-level data ($\pm 2\sigma$) (blue[24], green[25], red[26], black[27]); **c**, a global benthic foraminiferal $\delta^{18}O$ stack[19] (pink); **d**, benthic foraminiferal $\delta^{18}O$ record (five-point running mean) from marine core MD95-2042 (ref. 5) (purple); **e**, $\delta^{18}O$ record (seven-point running mean) from EPICA Dronning Maud Land (EDML)[28] (blue) and $\delta D$ record (seven-point running mean) from EPICA Dome C (EDC)[29] (orange); and **f**, NGRIP $\delta^{18}O$ record (five-point running mean)[30] (green). The MD95-2042 $\delta^{18}O$ record is plotted here on the Greenland Ice Core Chronology (GICC05 (ref. 31) for 0–60 kyr BP, and on the NGRIP (2004) chronology[30] for 60–85 kyr BP, after synchronizing the co-registered (MD95-2042) planktonic foraminiferal $\delta^{18}O$ record with Greenland $\delta^{18}O$ variations. EDML $\delta^{18}O$ and EDC $\delta D$ are plotted on the EDML1/EDC3 timescale[32]. NGRIP $\delta^{18}O$ is plotted on the GICC05 timescale for 0–60 kyr BP, and on its original timescale for 60–122 kyr BP (ref. 30). RSL is less reliable for about 14–23 kyr BP because of poor sampling resolution through an aplanktonic interval, and is therefore not shown. Marine Isotope Stages and terminations I and II (TI, TII) are indicated at the top of the figure.
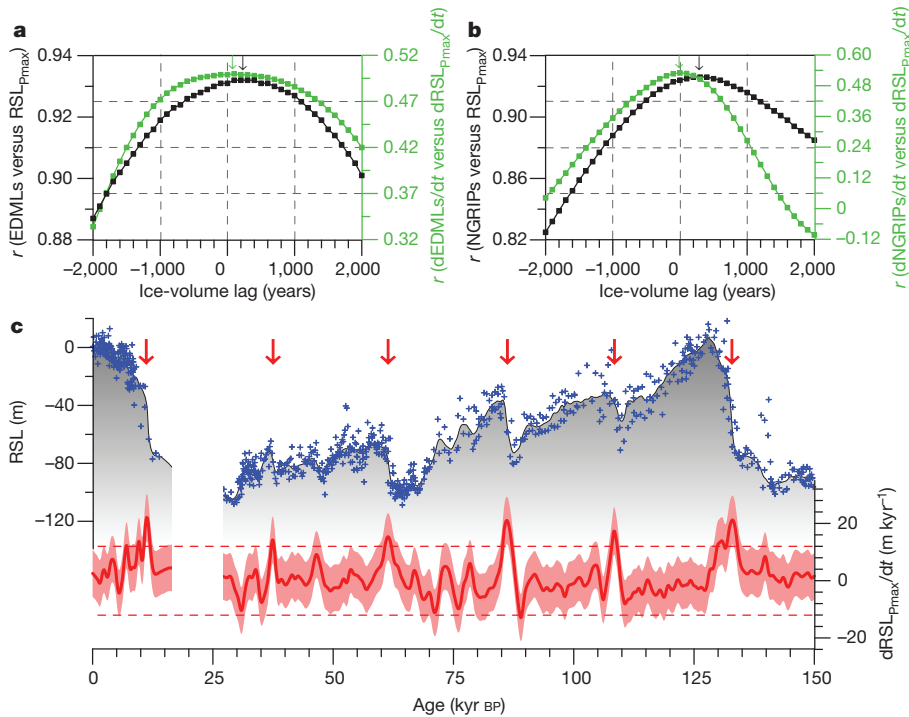


**Figure 3 | Lagged correlations of Antarctic and Greenland climate versus ice volume (sea-level), and rates of sea-level change over the last full glacial cycle. a**, **b**, Regression coefficients ($r$) (Supplementary Information) are plotted for the highest-probability sea-level curve and the smoothed (s) EDML and NGRIP $\delta^{18}O$ records (RSL$_{Pmax}$, EDMLs, NGRIPs; black squares, left-hand $y$ axes) and for their first derivatives (dRSL$_{Pmax}$/d$t$, dEDMLs/d$t$, dNGRIPs/d$t$; green squares; right-hand $y$ axes) for the regressions EDMLs versus RSL$_{Pmax}$ and dEDMLs/d$t$ versus dRSL$_{Pmax}$/d$t$ (**a**) and NGRIPs versus RSL$_{Pmax}$ and dNGRIPs/d$t$ versus dRSL$_{Pmax}$/d$t$ (**b**). Negative values of ice-volume lag correspond to changes in ice volume leading changes in polar climate. Optimum correlations are indicated (black and green arrows). **c**, RSL$_{Pmax}$ (grey shading), RSL data (blue crosses) and probability maximum of the first derivative of RSL (red) with 95% confidence interval (pink shading). Rates of sea-level change of +12 and −8 m kyr$^{-1}$ are indicated (dashed lines). Red arrows mark peaks in sea-level rises of more than 12 m kyr$^{-1}$ at 10.9–11.8 kyr BP, 37.4–37.5 kyr BP, 61.2–61.6 kyr BP, 85.5–86.9 kyr BP, 108.1–108.8 kyr BP and 132.1–133.8 kyr BP. Data from the Red Sea aplanktonic interval (about 14–23 kyr BP) are omitted.

Supplementary Information). We infer that Greenland climate closely tracks and/or is directly coupled with ice-volume changes, whereas Antarctic climate variability may lead ice-volume changes by up to 700 years (Supplementary Information).

Our new RSL chronology permits the first robust calculation of rates of relative sea-level change throughout the past 150,000 years (Fig. 3c). This reveals that rates of sea-level rise reached at least 1.2 m per century during all major phases of ice-volume reduction, and were typically up to 0.7 m per century (possibly higher, given the smoothing in our method) when sea-level exceeded 0 m during the LIG (Fig. 3c); the latter is consistent with independent estimates[21,22]. Rates of sea-level lowering rarely exceeded 0.8 m per century. Any differences between rates of change in ESL and RSL at Hanish Sill are likely to be captured within our uncertainties.

We have characterized and dated a continuous record of ice-volume variability throughout the last glacial cycle in a manner that is entirely independent of assumptions about the orbital insolation forcing of climate or about glaciological processes. We have also shown that, on suborbital timescales, polar climate and ice-volume changes were closely coupled in a quasi-direct phase relationship (within centuries). Our analyses hint that Antarctic climate change leads global ice-volume change by several centuries, which is a realistic timescale for ice-sheet adjustments[23]. Greenland climate, however, is found to change virtually simultaneously with ice volume, which may suggest a link of Greenland temperature to ice-volume change in the Northern Hemisphere through albedo feedback.

## METHODS SUMMARY

For the Soreq Cave record, we present 440 new U–Th datings that were acquired by multi-collector inductively coupled plasma mass spectrometry at the Geological Survey of Israel (Supplementary Information). Sample ages were corrected for detrital $^{230}$Th if $^{230}$Th/$^{232}$Th activity ratios were less than 160; for $^{230}$Th/$^{232}$Th activity ratios of more than 160–200 the correction factor was well within age uncertainties. Typical age uncertainties ($2\sigma$) are less than 1 kyr (0–35 kyr BP), less than 1.5 kyr (35–70 kyr BP), less than 2.5 kyr (70–120 kyr BP) and less than 4 kyr (120–160 kyr BP). Dating methods are further described in Supplementary Information. We applied Bayesian age modelling[15] to all U–Th datings ($\pm 2\sigma$), which typically reduced uncertainties to less than 0.5 kyr (0–60 kyr BP), less than 1 kyr (60–90 kyr BP) and less than 2 kyr (90–160 kyr BP) and had only minor impacts on absolute ages (generally less than 250 and less than 750 years for 0–70 and 70–160 kyr BP, respectively).

For the eastern Mediterranean record, continuous u-channel samples from the pristine archive half of core LC21 (35° 40′ N, 26° 35′ E; cruise MD81) were sub-sampled at 1-cm intervals. Stable isotope analyses of about 15–30 cleaned, similar-sized tests of G. ruber (white form) and N. pachyderma (dextral) from the greater than 300-μm and 150–300-μm sieved sediment fractions, respectively, were performed at the National Oceanography Centre, Southampton, on a Europa Geo2020 mass spectrometer fitted with an individual acid-bath carbonate preparation line. Standards (NBS-19 and an in-house Carrara marble) were run every 17 samples; external precision is less than 0.06‰.

1. Siddall, M. et al. Sea-level fluctuations during the last glacial cycle. Nature 423, 853–858 (2003).
2. Rohling, E. J. et al. Antarctic temperature and global sea level closely coupled over the past five glacial cycles. Nature Geosci. 2, 500–504 (2009).
3. Hansen, J. et al. Climate change and trace gases. Phil. Trans. R. Soc. A 365, 1925–1954 (2007).
4. Köhler, P. et al. What caused Earth's temperature variations during the last 800,000 years? Data-based evidence on radiative forcing and constraints on climate sensitivity. Quat. Sci. Rev. 29, 129–145 (2010).
5. Shackleton, N. J., Hall, M. A. & Vincent, E. Phase relationships between millennial-scale events 64,000–24,000 years ago. Paleoceanography 15, 565–569 (2000).
6. Waelbroeck, C. et al. Sea-level and deep water temperature changes derived from benthic foraminifera isotopic records. Quat. Sci. Rev. 21, 295–305 (2002).
7. Bintanja, R., van de Wal, R. S. W. & Oerlemans, J. Modelled atmospheric temperatures and global sea levels over the past million years. Nature 437, 125–128 (2005).
8. Cuffey, K. M. & Marshall, S. J. Substantial contribution to sea-level rise during the last interglacial from the Greenland ice sheet. Nature 404, 591–594 (2000).
9. Otto-Bliesner, B. L. et al. Simulating Arctic climate warmth and icefield retreat in the Last Interglacial. Science 311, 1751–1753 (2006).
10. Bar-Matthews, M., Ayalon, A., Gilmour, M., Matthews, A. & Hawkesworth, C. J. Sea–land oxygen isotopic relationships from planktonic foraminifera and speleothems in the Eastern Mediterranean region and their implication for paleorainfall during interglacial intervals. Geochim. Cosmochim. Acta 67, 3181–3199 (2003).
11. Almogi-Labin, A. et al. Climatic variability during the last ~90 ka of the southern and northern Levantine Basin as evident from marine records and speleothems. Quat. Sci. Rev. 28, 2882–2896 (2009).
12. Rohling, E. J. Environmental controls on salinity and δ$^{18}$O in the Mediterranean. Paleoceanography 14, 706–715 (1999).
13. Manning, S. W. et al. Chronology for the Aegean Late Bronze Age 1700–1400 BC. Science 312, 565–569 (2006).
14. De Vivo, B. et al. New constraints on the pyroclastic eruptive history of the Campanian volcanic plain (Italy). Mineral. Petrol. 73, 47–65 (2001).
15. Bronk Ramsey, C. Deposition models for chronological records. Quat. Sci. Rev. 27, 42–60 (2008).
16. Stanford, J. D. et al. Sea-level probability for the last deglaciation: a statistical analysis of far-field records. Global Planet. Change 79, 193–203 (2011).
17. Trommer, G. et al. Sensitivity of Red Sea circulation to sea level and insolation forcing during the last interglacial. Clim. Past 7, 941–955 (2011).
18. Lambeck, K. et al. Sea level and shoreline reconstructions for the Red Sea: isostatic and tectonic considerations and implications for hominin migration out of Africa. Quat. Sci. Rev. 30, 3542–3574 (2011).
19. Lisiecki, L. E. & Raymo, M. E. A Plio-Pleistocene stack of 57 globally distributed benthic δ$^{18}$O records. Paleoceanography 20, PA1003, doi:10.1029/2004PA001071 (2005).
20. Dansgaard, W. et al. Evidence for general instability of past climate from a 250-kyr ice-core record. Nature 364, 218–220 (1993).
21. Kopp, R. E., Simons, F. J., Mitrovica, J. X., Maloof, A. C. & Oppenheimer, M. Probabilistic assessment of sea level during the last interglacial stage. Nature 462, 863–868 (2009).
22. Thompson, W. G., Curran, H. A., Wilson, M. A. & White, B. Sea-level oscillations during the last interglacial highstand recorded by Bahamas corals. Nature Geosci. 4, 684–687 (2011).
23. Gregory, J. M., Huybrechts, P. & Raper, S. C. B. Threatened loss of the Greenland ice-sheet. Nature 428, 616 (2004).
24. Chappell, J. Sea level changes forced ice breakouts in the Last Glacial cycle: new results from coral terraces. Quat. Sci. Rev. 21, 1229–1240 (2002).
25. Cutler, K. B. et al. Rapid sea-level fall and deep-ocean temperature change since the last interglacial period. Earth Planet. Sci. Lett. 206, 253–271 (2003).
26. Thompson, W. G. & Goldstein, S. L. Open-system coral ages reveal persistent suborbital sea-level cycles. Science 308, 401–404 (2005).
27. Dutton, A. & Lambeck, K. Ice volume and sea level during the last interglacial. Science 337, 216–219 (2012).
28. EPICA Community Members. One-to-one coupling of glacial climate variability in Greenland and Antarctica. Nature 444, 195–198 (2006).
29. Jouzel, J. et al. Orbital and millennial Antarctic climate variability over the past 800,000 years. Science 317, 793–797 (2007).
30. North Greenland Ice Core Project Members. High-resolution record of Northern Hemisphere climate extending into the last interglacial period. Nature 431, 147–151 (2004).
31. Svensson, A. et al. A 60 000 year Greenland stratigraphic ice core chronology. Clim. Past 4, 47–57 (2008).
32. Parrenin, F. et al. The EDC3 chronology for the EPICA Dome C ice core. Clim. Past 3, 485–497 (2007).